Available online at www.sciencedirect.com
ScienceDirect
International Journal of Heat and Mass Transfer 50 (2007) 3244–3249
International Journal of HEAT and MASS TRANSFER
www.elsevier.com/locate/ijhmt

Technical Note

The effect of local thermal non-equilibrium on impulsive conduction in porous media

Ali Nouri-Borujerdi [a,*], Amin R. Noghrehabadi [a,b], D. Andrew S. Rees [b]

[a] School of Mechanical Engineering, Sharif University of Technology, Tehran, Iran
[b] Department of Mechanical Engineering, University of Bath, Bath BA2 7AY, UK

Received 13 July 2006
Available online 27 March 2007

Abstract

We examine the effect of local thermal non-equilibrium on the evolution of the stagnant temperature field in a semi-infinite porous medium. When local thermal equilibrium pertains, the temperature field which is induced by a step change in the temperature of a plane boundary is given by the classical conduction solution involving the complementary error function. When thermal local equilibrium does not apply, then conduction takes place more rapidly in one phase than in the other, although local thermal equilibrium is always approached as time increases. This note examines the evolution of the temperature field in each phase in detail using numerical methods, and the numerical solutions are supplemented by asymptotic solutions valid for both small and large times.

Keywords: Local thermal non-equilibrium; Conduction; Porous media; Impulsive heating

1. Introduction

An excellent review of conductive effects in a stagnant porous medium may be found in Cheng and Hsu [1]; in their chapter these authors consider periodic media and their aim is to determine the effective thermal conductivity of the combined medium in terms of the conductivities of the constituent phases. Therefore Cheng and Hsu provide important information for those wishing to use a single temperature field to model a two-phase saturated porous medium, or equivalently a composite solid consisting of two different constituents. However, there are situations where it is essential that the phases of a porous medium are modelled separately, and therefore the adoption of a two-temperature model has now become quite commonplace for convecting flows in porous media. Situations where two temperature fields are required are known either as LTNE (local thermal non-equilibrium) or, in the more linguistically pleasing form as LaLoThEq (lack of local thermal equilibrium). Schumann [2] was the first author to consider LTNE in porous media, although thermal diffusion was neglected in the model equations. The numerical study by Combarnous [3] predated by a couple of decades further work on fully nonlinear convection using this model. A recent review by Rees and Pop [4] summarises much of the present knowledge, including the various models used for LTNE and their application to free, mixed and forced convective flows and stability analyses; the reader is referred to this chapter for an overview of the topic.

Despite the now large volume of published works on convection using the two-temperature model, little is known about unsteady conduction in such systems. Carslaw and Jaeger [5] present the classic complementary error function solution for the conduction field which ensues after the temperature of a plane boundary of an isotropic conducting solid is raised suddenly to a new uniform level. However, when the conducting region consists of two phases, then conduction will usually occur more rapidly in one phase than in the other. For example, should the composite medium consist of alternating (i.e. striped) phases where the planar interfaces between the phases are

* Corresponding author.
E-mail address: anouri@sharif.edu (A. Nouri-Borujerdi).

0017-9310/$ - see front matter © 2007 Elsevier Ltd. All rights reserved.
doi:10.1016/j.ijheatmasstransfer.2006.12.016

Nomenclature

c	specific heat
h	inter-phase heat transfer coefficient
H	non-dimensional inter-phase heat transfer coefficient
k	thermal conductivity
L	length scale
q	surface rate of heat transfer in terms of η
T_f, T_s	fluid and solid temperatures, respectively
T_0	ambient temperature
T_1	surface temperature
$\underline{v}$	velocity vector
y	vertical coordinate

Greek symbols

α	diffusivity ratio
α_f, α_s	thermal diffusivity of the fluid and solid phases
γ	porosity-scaled conductivity ratio
ϵ	porosity
ζ	reseated similarity variable
η	similarity variable
θ	non-dimensional fluid temperature
ρ	density
τ	scaled time
ϕ	non-dimensional solid temperature
ω	non-dimensional diffusivity

Subscripts and superscripts

f	fluid
s	solid
$\wedge$	dimensional
η	derivative with respect to η
0, 1, 2	terms in power series
$\sim$	alternative scaling

aligned to be perpendicular to the heated surface, then heat will spread into the bulk of the medium more rapidly in the phase with the larger thermal diffusivity. Should one now consider these layers as being microscopic compared with the macroscopic lengthscales, then the macroscopic average temperature of each phase (as one would obtain on integrating over a representative elementary volume) will be different from the other. The present paper assumes that such a two-temperature model for conduction applies, and we consider how the complementary error function solution for the single phase system is altered by adopting the two-temperature model.

2. Governing equations

Nield and Bejan [6] quote the following equations as the simplest way in which LTNE may be modelled:

$$\epsilon(\rho c)_f \frac{\partial T_f}{\partial \hat{t}} + (\rho c)_f \underline{v} \cdot \nabla T_f = \epsilon \nabla \cdot (k_f \nabla T_f) + h(T_s - T_f), \quad (1)$$

$$(1-\epsilon)(\rho c)_s \frac{\partial T_s}{\partial \hat{t}} = (1-\epsilon)\nabla \cdot (k_s \nabla T_s) + h(T_f - T_s). \quad (2)$$

In these equations the various terms take their usual meanings with the subscripts, f and s, denoting fluid and solid, respectively. Thus T_f and T_s are intrinsic averages of the temperature fields, and this allows us to set $T_f = T_s = T_1$ on the boundary. The quantity ϵ is the porosity of the medium. We shall assume that there is no fluid flow, and hence the fluid velocity $\underline{v}$ is set to zero. Therefore the physical situation corresponds either to a porous medium where the bounding surface is horizontal (i.e. so that there is no induced flow), or to a composite medium consisting of two solids. Finally, the value h is a heat transfer coefficient which models the detailed microscopic transmission of heat between the phases.

The medium, which occupies the region $\hat{y} \geqslant 0$, is held at the temperature T_0 until $\hat{t} = 0$ whereupon the temperature at the $\hat{y} = 0$ boundary is raised suddenly to $T = T_1$. We may now non-dimensionalise Eqs. (1) and (2) using the following substitutions:

$$\hat{t} = \frac{L^2}{\alpha_f} t, \quad (\hat{x}, \hat{y}) = L(x, y), \quad T_f = T_0 + (T_1 - T_0)\theta,$$

$$T_s = T_0 + (T_1 - T_0)\phi, \quad (3)$$

where $\alpha_f = k_f/(\rho c)_f$ is the thermal diffusivity of the fluid phase, and L is a macroscopic lengthscale, details of which are expanded upon below. Therefore Eqs. (1) and (2) reduce to

$$\theta_t = \theta_{xx} + \theta_{yy} + H(\phi - \theta), \quad (4)$$

$$\alpha\phi_t = \phi_{xx} + \phi_{yy} + H\gamma(\theta - \phi). \quad (5)$$

In Eqs. (4) and (5) the non-dimensional parameters, α, H and γ are defined according to

$$\alpha = \frac{\alpha_f}{\alpha_s}, \quad H = \frac{hL^2}{\epsilon k_f}, \quad \gamma = \frac{\epsilon k_f}{(1-\epsilon)k_s}. \quad (6a, b, c)$$

These quantities are a diffusivity ratio, a scaled inter-phase heat transfer coefficient and a porosity-modified conductivity ratio. It is worth noting that it is also possible to remove H from this list of parameters since there is no natural lengthscale in such a 'deep pool' system, and therefore we could set $H = 1$ in (6b) to define the lengthscale $L = \sqrt{\epsilon k_f/h}$. An alternative means of removing H from the equations is by the use of the following transformations, which allow us to use the natural coordinate, η, as suggested by the classical conduction solution of Carslaw and Jaeger [5]:

$$\eta = \frac{y}{2\sqrt{t}}, \quad \tau = H\sqrt{t}. \tag{7a, b}$$

In addition we may set all x-derivatives to zero as conduction takes place solely in the y-direction. Hence Eqs. (4) and (5) reduce to

$$4\tau\theta_\tau = \theta_{\eta\eta} + 2\eta\theta_\eta + 4\tau(\phi - \theta), \tag{8}$$

$$4\alpha\tau\phi_\tau = \phi_{\eta\eta} + 2\alpha\eta\phi_\eta + 4\gamma\tau(\theta - \phi). \tag{9}$$

The boundary conditions are simply that $\theta = \phi = 1$ on $\eta = 0$ and that $\theta, \phi \to 0$ as $\eta \to \infty$. These equations have the property that the initial conditions are given uniquely by the ordinary differential equations which are obtained by setting $\tau = 0$ into Eqs. (8) and (9).

It is important to note that should the bounding surface $\hat{y} = 0$ corresponds to a horizontal surface, then the thermal front we compute below will develop solely in the vertical direction, and therefore the absence of buoyancy forces on the macroscopic scale leads naturally to no flow. When the bounding surface is inclined, then the induced velocity along the surface may be shown to be proportional to the θ-profile when Darcy's law applies, but this induced flow does not affect the developing temperature profiles.

3. Solutions at early times

At early times it is possible to determine a power series solution of Eqs. (8) and (9) as follows:

$$\begin{pmatrix}\theta\\ \phi\end{pmatrix} = \begin{pmatrix}\theta_0(\eta)\\ \phi_0(\eta)\end{pmatrix} + \tau\begin{pmatrix}\theta_1(\eta)\\ \phi_1(\eta)\end{pmatrix} + \tau^2\begin{pmatrix}\theta_2(\eta)\\ \phi_2(\eta)\end{pmatrix} + \cdots \tag{10}$$

At O(1) the solutions are

$$\theta_0 = \operatorname{erfc}(\eta), \quad \phi_0 = \operatorname{erfc}(\alpha^{0.5}\eta), \tag{11a, b}$$

and therefore the relative thickness of the thermal field in the two phases depends only on the diffusivity ratio. Thus, if the fluid phase has a higher thermal diffusivity, then $\alpha > 1$, and the thermal field of the fluid phase is more extensive. At this stage, then, it is only the value of α that determines the relative thicknesses of the two thermal boundary layers.

At O(τ) it is again possible to proceed easily analytically, and the temperatures are given by

$$\theta_1 = \frac{2\alpha\eta^2 + 1}{\alpha - 1}\left[\operatorname{erfc}(\eta) - \operatorname{erfc}\sqrt{\alpha}\eta\right] + \frac{2\sqrt{\alpha}}{\sqrt{\pi}(\alpha - 1)}\left[\eta e^{-\alpha\eta^2} - \sqrt{\alpha}\eta e^{-\eta^2}\right], \tag{12}$$

$$\phi_1 = \gamma\frac{2\eta^2 + 1}{\alpha - 1}\left[\operatorname{erfc}(\eta) - \operatorname{erfc}\sqrt{\alpha}\eta\right] + \frac{2\gamma}{\sqrt{\pi}\sqrt{\alpha}(\alpha - 1)}\left[\eta e^{-\alpha\eta^2} - \sqrt{\alpha}\eta e^{-\eta^2}\right]. \tag{13}$$

We note that both of these expressions become zero as $\alpha \to 1$ since, in that limit, the porous medium consists of two phases with identical properties, and the solutions given in (10) form the exact solution of Eqs. (8) and (9).

Analytical solutions for higher order terms are considerably more complicated and we reverted to a numerical solution for the O(τ^2) equations using a highly accurate fourth order Runge–Kutta scheme. Comparisons of these solutions with the numerical simulations of the full parabolic partial differential system, (8) and (9), are presented later.

4. Solutions at late times

As time progresses the expansion of the thermal field slows. As we expect the thermal boundary layer thickness in terms of y to be proportional to $t^{1/2}$ the speed of the developing thermal front is proportional to $t^{-1/2}$, which allows an increasing amount of time for the phases to reach a state of thermal equilibrium. Therefore we expect LTE to be achieved at late times. Mathematically we may appeal to Eqs. (8) and (9) by first setting τ to be asymptotically large and then by using a straightforward order-of-magnitude analysis to show that the final terms in these equations must dominate their respective equations, and hence that $\theta = \phi$ to leading order. More specifically, we may set

$$\begin{pmatrix}\theta\\ \phi\end{pmatrix} = \begin{pmatrix}\theta_0(\eta)\\ \phi_0(\eta)\end{pmatrix} + \tau^{-1}\begin{pmatrix}\theta_1(\eta)\\ \phi_1(\eta)\end{pmatrix} + \tau^{-2}\begin{pmatrix}\theta_2(\eta),\\ \phi_2(\eta)\end{pmatrix} + \cdots \tag{14}$$

into Eqs. (8) and (9) where θ_0 and ϕ_0 are equal. At leading order we obtain

$$\theta_0'' + 2\eta\theta_0' + 4(\phi_1 - \theta_1) = 0, \tag{15}$$

$$\phi_0'' + 2\alpha\eta\phi_0' + 4\gamma(\theta_1 - \phi_1) = 0. \tag{16}$$

The terms in θ_1 and ϕ_1 may be removed by multiplying Eq. (15) by γ and then adding Eq. (16). The resulting equation for θ_0 (or ϕ_0) then has solution

$$\theta_0 = \phi_0 = \operatorname{erfc}\left(\frac{\gamma + 1}{\gamma + \alpha}\right)^{0.5}\eta = \operatorname{erfc}\zeta, \tag{17}$$

where

$$\zeta = \eta/\omega, \tag{18}$$

and where

$$\omega^2 = \frac{\gamma + 1}{\gamma + \alpha} = \frac{[\epsilon k_f + (1 - \epsilon)k_s]/k_f}{[\epsilon(\rho C)_f + (1 - \epsilon)(\rho C)_s]/(\rho C)_f}. \tag{19}$$

At the next order it is possible to show that

$$\theta_1'' + 2\eta\theta_1' + 4\theta_1 + 4(\phi_2 - \theta_2) = 0, \tag{20}$$

$$\phi_1'' + 2\alpha\eta\phi_1' + 4\alpha\phi_1 + 4\gamma(\theta_2 - \phi_2) = 0. \tag{21}$$

Eq. (15) shows that

$$\phi_1 = \theta_1 - \frac{1}{4}[\theta_0'' + 2\eta\theta_0'] = \theta_1 + \frac{1}{4}(\omega^2 - 1)\theta_0'', \tag{22}$$

which may be used in (20) and (21) when eliminating θ_2 and ϕ_2 between those equations, to yield the following equation for θ_1:

$$\omega^2\theta_1'' + 2\eta\theta_1' + 4\theta_1 = \frac{(\omega^2-1)(\alpha\omega^2-1)}{4(\alpha+\gamma)}\theta_0''''. \tag{23}$$

This equation has the analytical solution

$$\theta_1 = -\frac{(\omega^2-1)(\alpha\omega^2-1)}{4(\alpha+\gamma)}\frac{4}{\sqrt{\pi}}\zeta^3 e^{-\zeta^2} + C\zeta e^{-\zeta^2}, \tag{24}$$

where C is an arbitrary constant, and where, for convenience, the solution has been written out in terms of ζ, rather than η. The term multiplying C is a complementary function which satisfies all the appropriate homogeneous boundary conditions, and therefore its amplitude is indeterminate. This means that it is not possible to present a second term in the large-τ expansion, unless its value is estimated by comparison with the fully numerical solution presented below.

5. Numerical solutions

For intermediate values of τ the system given by (8) and (9) was solved using the Keller box method, a new well-known implicit scheme which is closely related to the Crank Nicholson method, except that the governing equations are reduced to a first order form in η, rather than kept in second order form. In the present paper we used 100 equally spaced intervals between $\eta = 0$ and $\eta = 10$. Central differences in τ were employed. Grid refinement tests indicated that our solutions are accurate to at least three significant figures.

Fig. 1 displays an example comparison between the numerical solution for the case $\alpha = 2$ and $\gamma = 1$ and the asymptotic solutions for both small and large values of τ. This comparison uses the surface rates of heat transfer (i.e. $q_f = -\theta'(\eta = 0)$ and $q_s = -\phi'(\eta = 0)$) as the measures of the evolving temperature profiles of the two phases.

At early times it is clear to see that the leading terms given in (11) are highly accurate when $\tau < 0.01$ but that the temperatures of the individual phases begin to affect one another after that time. Also shown are the corresponding early time curves using both two and three terms. These graphs show that there is little to be gained by including a third term, and that the adoption of a two-term expansion yields solutions which are highly accurate until $\tau = 0.1$. Thereafter one must rely on the fully numerical simulation.

At late times, which, for the present parameter set means $\tau > 100$, the temperatures of the different phases are no longer distinguishable graphically and that the late-time asymptotic solution given in (16) now applies with a high degree of accuracy.

Fig. 2 displays the variation of the surface rates of heat transfer with τ for $\gamma = 1$ for a set of values of α. The continuous lines depict the fluid phase while the broken lines

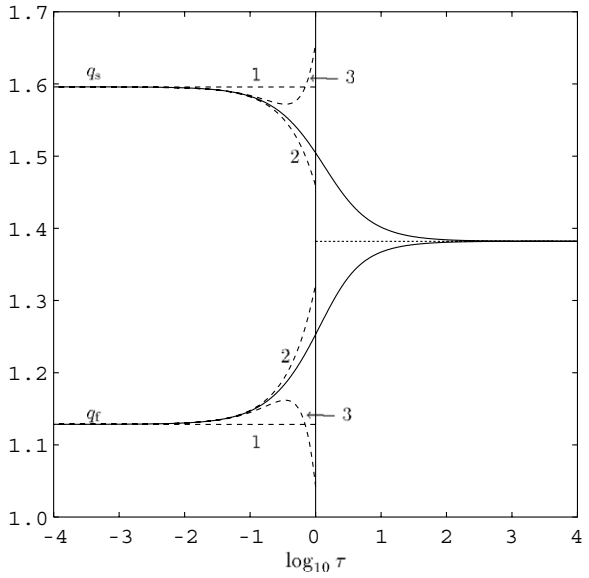

Fig. 1. Comparison between the numerical asymptotic variations of the surface rates of heat transfer, q_f and q_s as a function of $\log_{10}\tau$ for $\alpha = 2$ and $\gamma = 1$. The fully numerical solutions are depicted as continuous curves, the small-time asymptotic solutions as long dashes and the long-time asymptotic solution as short dashes. One, two and three terms of the short-time asymptotic solution are shown.

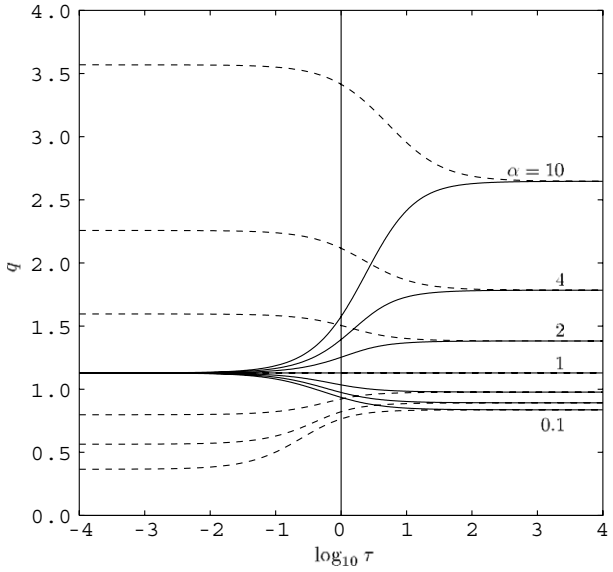

Fig. 2. Evolution with $\log_{10}\tau$ of q_f (continuous curves) and q_s (dashed curves) for $\gamma = 1$, and for $\alpha = 0.1, 0.25, 0.5, 1, 2, 4$ and 10.

depict the solid phase. At early times all the fluid phase curves are coincident, which is consistent with (11), while the solid phase curves correspond to a rate of heat transfer which is proportional to $\sqrt{\alpha}$, which is again consistent with (11). Once more, at large times, the respective fluid and solid phase curves for any chosen parameter set become coincident (i.e. LTE is achieved) as τ increases, although the time at which this happens increases with increasing α. We note that when $\alpha = 1$ the phases have identical temperatures at all times and they are given by $\theta = \phi = \mathrm{erfc}(\eta)$.

Figs. 3 and 4 correspond to $\alpha = 0.5$ and $\alpha = 2$, respectively, each for a choice of values of γ varying from 0.01 to 100. In both cases, when $\gamma = 100$ the large-time asymptotic solution is very nearly erfc (η), which is the small-time leading order solution, and therefore the rate of heat transfer within the fluid phase hardly changes with time. In like fashion, when $\gamma = 0.01$, the heat transfer within the solid phase changes little since Eqs. (17) and (11b) are almost identical.

At this point it is important to note that the non-dimensionalisation used for time in Eq. (3) was based upon the diffusivity of the fluid, and it does not represent the usual way in which non-dimensionalisation is carried out when the single energy equation model is used. If we replace the scaling for $\hat{t}$ used in (3) by

$$\hat{t} = \frac{L^2}{\omega^2 \alpha_f} \tilde{t}, \tag{25}$$

where ω is given by (19) and

$$\tilde{\tau} = H\sqrt{\tilde{t}} \tag{26}$$

(c.f. Eq. (7b)), then Eqs. (8) and (9) become

$$4\tilde{\tau}\left(\frac{\gamma+1}{\gamma+\alpha}\right)\theta_{\tilde{\tau}} = \theta_{\eta\eta} + 2\eta\left(\frac{\gamma+1}{\gamma+\alpha}\right)\theta_{\eta} + 4\tilde{\tau}(\phi - \theta), \tag{27}$$

$$4\alpha\tilde{\tau}\left(\frac{\gamma+1}{\gamma+\alpha}\right)\phi_{\tilde{\tau}} = \phi_{\eta\eta} + 2\alpha\left(\frac{\gamma+1}{\gamma+\alpha}\right)\eta\phi_{\eta} + 4\gamma\tilde{\tau}(\theta - \phi). \tag{28}$$

Eqs. (27) and (28) may be shown to have the following symmetry properties,

$$\theta(\eta, \tilde{\tau}, \gamma, \alpha) = \phi(\eta, \tilde{\tau}\gamma^{-1}, \gamma^{-1}, \alpha^{-1}), \tag{29a}$$

$$\phi(\eta, \tilde{\tau}, \gamma, \alpha) = \phi(\eta, \tilde{\tau}\gamma^{-1}, \gamma^{-1}, \alpha^{-1}), \tag{29b}$$

although this symmetry is lost in the presence of fluid flow.

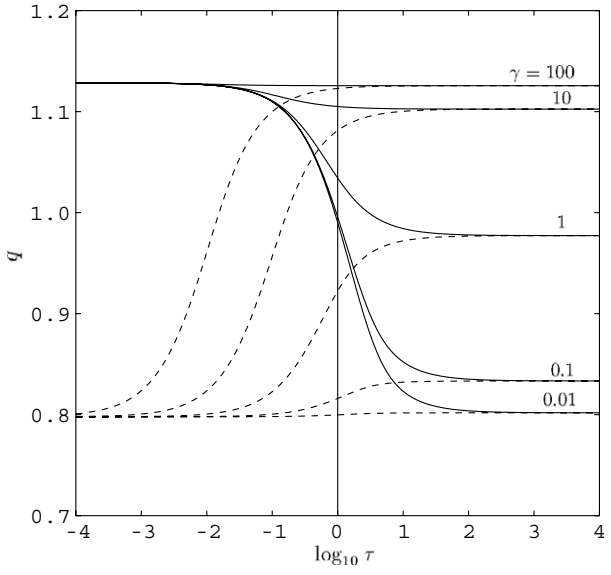

Fig. 3. Evolution with $\log_{10}\tau$ of q_f (continuous curves) and q_s (dashed curves) for $\alpha = 0.5$, and for $\gamma = 0.01, 0.1, 1, 10$ and 100.

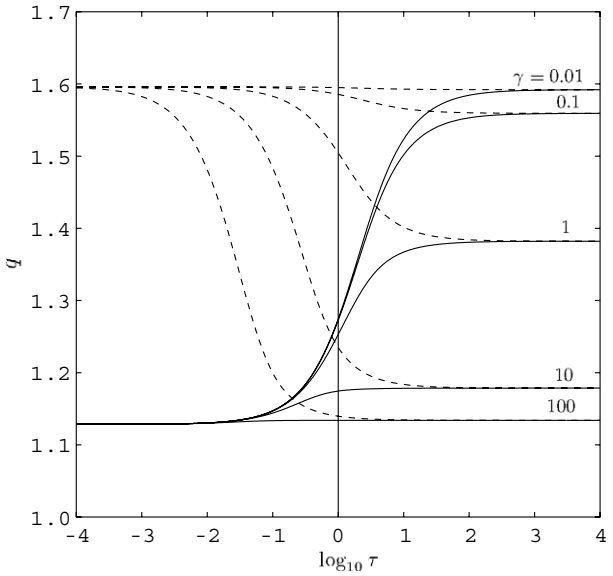

Fig. 4. Evolution with $\log_{10}\tau$ of q_f (continuous curves) and q_s (dashed curves) for $\alpha = 2$, and for $\gamma = 0.01, 0.1, 1, 10$ and 100.

In this alternative reseating both phases tend towards erfc(η) for large values of $\tilde{\tau}$. This is seen clearly in Fig. 5 where $\gamma = 1$ and a small selection of values of α are represented. The leading order small-time solutions are now given by

$$\theta \sim \mathrm{erfc}\left[\left(\frac{\gamma+1}{\gamma+\alpha}\right)^{0.5}\eta\right] = \mathrm{erfc}(\omega\eta), \tag{30a}$$

$$\phi \sim \mathrm{erfc}\left[\left(\alpha\frac{\gamma+1}{\lambda+\alpha}\right)^{0.5}\eta\right] = \mathrm{erfc}(\sqrt{\alpha}\omega\eta). \tag{30b}$$

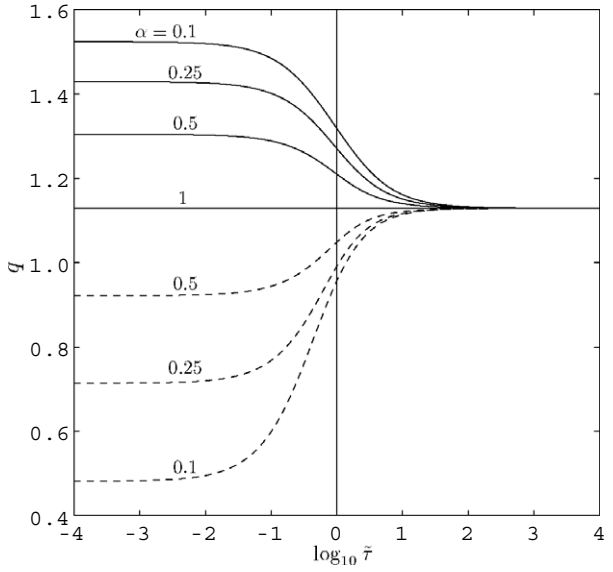

Fig. 5. Evolution with $\log_{10}\tilde{\tau}$ of q_f (continuous curves) and q_s (dashed curves) for $\gamma = 1$, and for $\alpha = 0.1, 0.25, 0.5$ and 1. The q_f and q_s curves are identical when $\gamma = 1$.

The corresponding curves for $\alpha > 1$ are virtually identical to those given in Fig. 5 except that the roles of the phases axe interchanged and that the α values represented in Fig. 5 become their respective reciprocals.

Finally, we note that the chief effect of this rescaling of time is to shift the q-curves both vertically and horizontally as compared with those given in Figs. 2–4 and therefore, for the sake of brevity, we omit the presentation of further curves.

6. Conclusions

In this note we have considered the evolution of the temperature field in a stagnant porous medium which is suddenly heated from below and where local thermal non-equilibrium effects are significant. At early times the classical complementary error function for a uniform single-phase medium applies in each phase, but the thermal boundary layer thicknesses depend on the value of α, the diffusivity ratio. At later times, as the progress of the thermal front slows down, the temperatures of the phases are found to tend towards the same profile as one another; this is when local thermal equilibrium is achieved. The time at which LTE is achieved clearly depends on the value of H given the definition of τ in Eq. (7) However it also depends on the values of γ and α. LTE is achieved relatively early for larger values of γ, but the value of τ at which this happens varies over many orders of magnitude as γ is varied.

It is now our intention to examine the solutions presented above for their stability characteristics. When heated from below the present system has the potential for thermo-convective instability since relatively heavy fluid overlies relatively light fluid. In related studies using a single energy equation (i.e. where LTE has been assumed), Selim and Rees [7–9] have studied various linear and nonlinear stability characteristics of the evolving temperature field. We shall determine how this scenario is altered in the presence of LTNE.

Acknowledgements

The second author (A.R.N.) wishes to express his cordial thanks to the British Council for financial support for his visit to the University of Bath, and to the University of Bath for their hospitality.

References

[1] P. Cheng, C.T. Hsu, in: D.B. Ingham, I. Pop (Eds.), Heat conduction, Transport Phenomena in Porous Media I, Pergamon, 1998, pp. 57–76.
[2] T.E.W. Schumann, Heat transfer; a liquid flowing through a porous prism, J. Franklin Inst. 208 (1929) 405–416.
[3] M. Combarnous, Description du transferte de chaleur par convection naturelle dans une couche poreuse horizontale à l'aide d'un coefficient de transfert solide–fluide, C.R. Acad. Sci. Paris II A 275 (1972) 1375–1378.
[4] D.A.S. Rees, I. Pop, in: D.B. Ingham, I. Pop (Eds.), Local thermal nonequilibrium in porous medium convection, Transport Phenomena in Porous Media III, Pergamon, 2005, pp. 147–173.
[5] H.S. Carslaw, J.C. Jaeger, Conduction of Heat in Solids, Oxford University Press, 1986.
[6] D.A. Nield, A. Bejan, Convection in Porous Media, third ed., Springer Verlag, New York, 2006.
[7] A. Selim, D.A.S. Rees, The instability of a developing thermal front in a porous medium. I. Linear theory, J. Porous Media, in press.
[8] A. Selim, D.A.S. Rees, The instability of a developing thermal front in a porous medium. II. Nonlinear evolution, J. Porous Media, in press.
[9] A. Selim, D.A.S. Rees, Secondary instabilities of a developing thermal front in a porous medium, Paper PRT-03, in: Proceedings of the 13th International Heat Transfer Conference, August 12–18, Sydney, Australia, 2006.